Sinusoidal-flux reluctance machine driven with three-phase inverter for improving power density with reduced torque and input current ripples

Masaki Iida, Kazuhiro Umetani, Takayuki Kusumi, Masataka Ishihara, and Eiji Hiraki
Graduate school of natural science and technology,
Okayama University,
Okayama, Japan

Published in: 2021 23rd European Conference on Power Electronics and Applications (EPE'21 ECCE Europe)

DOI: 10.23919/EPE21ECCEEurope50061.2021.9570573

Sinusoidal-Flux Reluctance Machine Driven with Three-Phase Inverter for Improving Power Density with Reduced Torque and Input Current Ripples

Masaki Iida, Kazuhiro Umetani, Takayuki Kusumi, Masataka Ishihara, Eiji Hiraki
Okayama University / Graduate School of Natural Science and Technology
3-1-1 Tsushimanaka, Kita-ku, Okayama, Japan
Tel.: +81 / (86) – 251.8121.
Fax: +81 / (86) – 251.8115.
E-Mail: pk228e77@s.okayama-u.ac.jp

Keywords

«Switched reluctance drive», «Electrical machine», «Ripple minimization», «Synchronous Reluctance Machine (SynRM) ».

Abstract

Reluctance machines such as the switched reluctance machines (SRMs) and the synchronous reluctance machines (SynRMs) are recently investigated for propulsion motors of the electrified vehicles owing to their robust mechanical construction, high thermal tolerance, and cost-competitiveness. However, practical application of the reluctance machines to the vehicle propulsion has been hindered by the fact that the conventional SRMs and SynRMs are difficult to meet all the three preferable features for the vehicular application: 1. High power density, 2. Low torque and input-current ripples, 3. Being drivable by the normal three-phase inverter. This paper addresses this issue by proposing a novel reluctance machine. The prominent features of the proposed reluctance machine are the sinusoidal reluctance profile and the delta-connected phase windings, both of which differ from conventional reluctance machines. Along with the theoretical discussion of the basic operating principles of the proposed reluctance machines, this paper presents a simple performance estimation of the proposed machine, the SRM, and the SynRM, which supported that the proposed machine can meet the three preferable features. Furthermore, the experiment successfully supported the operating principles of the proposed machine, suggesting the feasibility of the proposed machine for vehicle applications.

Introduction

Recently, the worldwide concern of global warming has given rise to the electrified vehicles, such as electric vehicles and hybrid vehicles, for reduction of the carbon dioxide emission. The vehicle propulsion needs to cover a wide range of torque and rotation speed. Therefore, the majority of the electrified vehicles utilize the permanent magnet synchronous machines (PMSM) [1]–[3] as the propulsion motors because they can offer large torque at comparatively small rotation speed. However, the PMSMs contain permanent magnets, which are expensive, mechanically fragile, and thermally degradable. Therefore, the electrified vehicles with the PMSMs suffer from the high cost of the motor and need for the special care to protect the motor from mechanical vibration and excessive heat-up. These drawbacks are hindering the electrification of low-cost cars, thus becoming great obstacles for further widespread of the electrified vehicles.

The reluctance machines can be a key technology to overcome these obstacles. The reluctance machines are free from the permanent magnets and therefore are attractive owing to their simple but robust mechanical construction, high thermal tolerance, and strong cost-effectiveness. Owing to their benefits, researchers are recently investigating the application of the reluctance machines to vehicular propulsion [4]–[11]. Two typical reluctance machines have been commonly investigated for the vehicular application: One is the synchronous reluctance machine (SynRM) [8], [10], [11]; the other is the switched reluctance machine (SRM) [6], [7], [9].

The SynRMs are the reluctance machine having the sinusoidal phase inductance profile and driven by the sinusoidal phase current [12]. The SynRMs are known to exhibit small input torque ripple, which is an important feature for vehicle propulsion to offer high driving comfort, and small input current ripple, which is also an important feature to protect the battery from deterioration of the lifetime. Furthermore, as illustrated in Fig. 1(a), the SynRM can be driven with the three-phase inverter, which is the most widely utilized inverter topology in various industry and therefore can be supplied at a moderate cost. However, the SynRM tends to suffer from low power density due to small maximum output torque and therefore is difficult for vehicular application, which needs to cover a wide operating range of the torque.

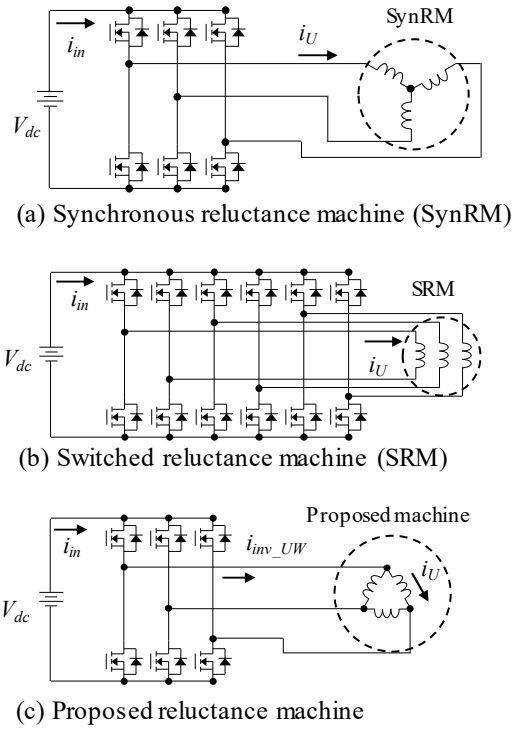

(a) Synchronous reluctance machine (SynRM)

(b) Switched reluctance machine (SRM)

(c) Proposed reluctance machine

Fig. 1: Driving systems of 3 reluctance machines

Meanwhile, the SRMs are the reluctance machine having the triangular phase inductance profile and driven by the step-like phase current waveform. The SRMs are reported to exhibit comparatively larger output power than SynRM, particularly at a low rotation speed. However, the SRMs tend to suffer from large torque ripple and large input current ripple [13]. Furthermore, the SRM cannot be driven with the three-phase inverter as illustrated in Fig. 1(b) because the sum of the phase current of all the phases is not zero. Certainly, the recent studies have proposed the driving methods of the SRMs that can reduce the torque and input-current ripples [14][15]. However, these methods still have difficulty in driving the SRMs with the three-phase inverters.

As seen above, the conventional reluctance machines have drawbacks that hinder the vehicular application of the reluctance machines. The purpose of this paper is to propose a novel reluctance machine that can improve the maximum output power compared to the SynRM but still has the small torque and input-current ripples and can be driven with the three-phase inverter as illustrated in Fig. 1(c). As discussed in the next section, the phase flux waveform of SynRM contains the third harmonics. This harmonic leads to an increase in the peak magnetic flux density, thus decreasing the maximum output power. Therefore, to solve this problem, the proposed reluctance machine is designed to be driven by the sinusoidal phase flux waveform.

The remainder of this paper is divided in four sections. Section II briefly reviews the SynRM and the SRM. Then, section III discusses the basic operating principles of the proposed reluctance machine in comparison with the SynRM and the SRM. Sections IV and V perform the simulation and the experiment, respectively, to confirm the operating principles of the proposed reluctance machine. Finally, section IV gives the conclusions.

Brief Review of SynRM and SRM

This subsection briefly reviews the SynRM and the SRM to discuss the causes of their drawbacks in vehicle propulsion. These machines are assumed to have the three phases of the concentrated windings and to be free from the magnetic saturation for simplification of the discussion.

Figure 2 shows the inductance profile, the phase current waveform, the magnetic flux of the SynRM, respectively. The SynRM is designed to have the sinusoidal inductance profile and is driven with the sinusoidal phase current. The inductance profile has twice as large wavenumber as the phase current. Therefore, by taking the origin of the electric angle at the maximum inductance, the inductance profile and the phase current can be expressed as

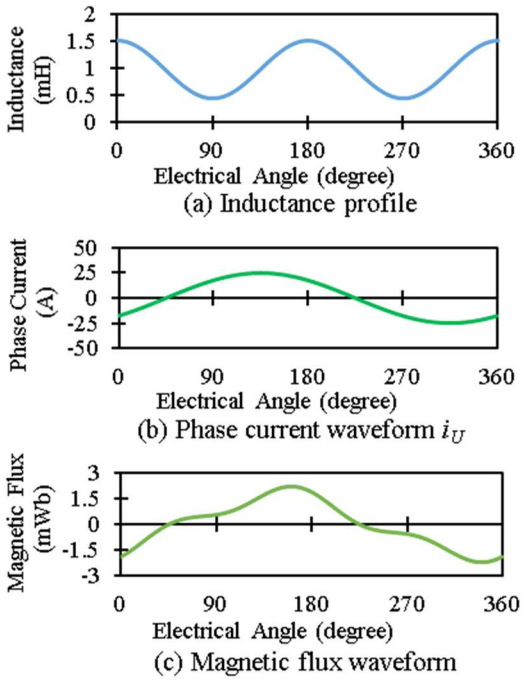

Fig. 2: Operating waveforms of SynRM

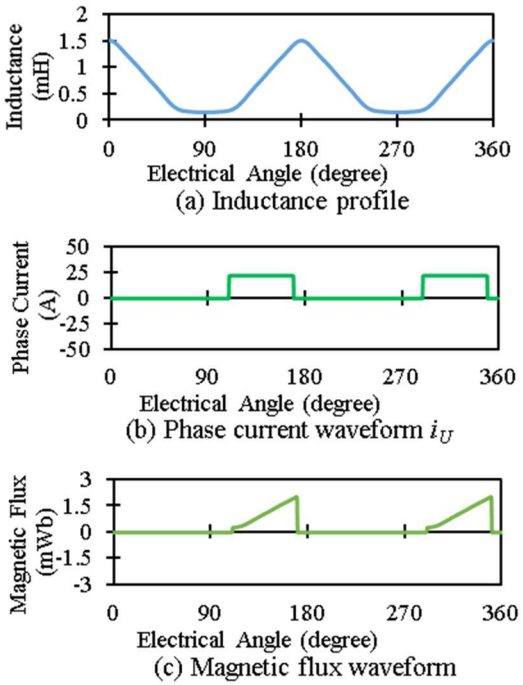

Fig. 3: Operating waveforms of SRM

$$L_U = \frac{L_{\max} + L_{\min}}{2} + \frac{L_{\max} - L_{\min}}{2}\cos 2\theta, \quad i_U = A_s \cos\theta + B_s \sin\theta, \tag{1}$$

where L is the phase inductance, θ is the electric angle, i is the phase current, subscription U indicates phase U, L_{max} and L_{min} are the maximum and minimum values of the phase inductance, A_s and B_s are the parameters determining the amplitude and phase of the phase current.

The instantaneous torque τ and the input current i_{in} of a reluctance machine can be formulated according to [16] as

$$\tau = \sum_{k=U,V,W} \frac{P}{2}\frac{dL_k}{d\theta} i_k^2, \quad i_{in} = \frac{1}{V_{dc}} \sum_{k=U,V,W} v_k i_k = \frac{1}{V_{dc}} \sum_{k=U,V,W} \frac{dL_k i_k}{dt} i_k = \frac{\Omega}{V_{dc}} \sum_{k=U,V,W} \left(2\tau + \frac{PL_k}{2}\frac{di_k^2}{d\theta} \right). \tag{2}$$

where P is the number of the rotor pole pairs; V_{dc} is the voltage of the DC power supply to the inverter; v is the phase voltage; Ω is the angular velocity of the rotor; subscriptions V and W indicates phase V and W, respectively. Substituting (1) into (2) results in the following equations, which indicates the constant torque and the constant input current regardless of the electric angle.

$$\tau = -\frac{3P}{4}(L_{\max} - L_{\min})A_s B_s, \quad i_{in} = -\frac{\Omega}{V_{dc}}\frac{3P}{4}(L_{\max} - L_{\min})A_s B_s. \tag{3}$$

Meanwhile, the phase flux ϕ_U is calculated according to $\phi_U = L_U i_U / N$, where N is the number of turns, as

$$\phi_U = \frac{3L_{\max} + L_{\min}}{4N} A_s \cos\theta + \frac{L_{\max} + 3L_{\min}}{4N} B_s \sin\theta + \frac{L_{\max} - L_{\min}}{4N} A_s \cos 3\theta + \frac{L_{\max} - L_{\min}}{4N} B_s \sin 3\theta. \tag{4}$$

Therefore, unlike the phase current, the phase flux contains the 3rd harmonics as shown in Fig. 2(c), which increases the peak value of the magnetic flux. Because the maximum acceptable flux induction is restricted by the magnetic saturation of the stator and rotor core, the 3rd harmonics in ϕ reduces the maximum output torque due to the increase in the peak magnetic flux.

On the other hand, the SRM has the triangular phase inductance profile and driven by the step-like phase current waveform, as depicted in Fig. 3. Ideally, the phase current waveform can be given as

$$i_U = I_{magn} \quad \text{if} \quad \theta_{fir} < \theta < \theta_{ext}, \quad \text{else} \quad i_U = 0, \tag{5}$$

where I_{magn} is the constant phase current during magnetization period, θ_{fir} and θ_{ext} are the firing and extinction angles. These angles are set so that the phase inductance has the constant slope $\partial L_U/\partial\theta$ during magnetization, i.e. in $\theta_{fir} < \theta < \theta_{ext}$. Then, the instantaneous torque and the instantaneous input current contributed by the phase become constant, according to (1). Therefore, by alternating the magnetization of the phases for 120 degrees with seamless commutation, the phase current waveform shown in Fig. 3 can ideally generate the constant torque and the constant input current

However, the phase flux waveform contains the sharp magnetization and demagnetization steps, which cannot be achieved due to the limited voltage applied to the phase winding. Consequently, an actual phase current waveform must deviate from the step-like waveform shown in Fig. 3, thus resulting in the large torque ripple and the input current ripple during the magnetizing and demagnetizing transient periods.

As seen in the above discussion, the drawbacks of these conventional reluctance machines originated from the phase flux waveforms containing the harmonics or the sharp steps. This implies that the performance improvement can be expected by developing the reluctance machine that can be driven with the sinusoidal phase flux waveform.

Proposed Reluctance Machine

The proposed reluctance machine is the reluctance machine driven with the sinusoidal phase flux waveform. Figure 4 shows the operating waveforms of the proposed reluctance machine. The proposed reluctance machine is designed to have the sinusoidal reluctance profile, unlike the sinusoidal inductance profile of the SynRM, with the wavenumber twice as large as the phase flux. Therefore, the reluctance profile and the phase flux can be expressed as

$$\begin{aligned} R_U &= \frac{R_{\max} + R_{\min}}{2} - \frac{R_{\max} - R_{\min}}{2}\cos 2\theta, \\ \phi_U &= A_p \cos\theta + B_p \sin\theta, \end{aligned} \tag{6}$$

where R is the phase reluctance, subscription U indicates phase U, R_{max} and R_{min} are the maximum and minimum values of the phase reluctance, A_p and B_p are the parameters determining the amplitude and phase of the phase flux.

Noting that R and ϕ can be expressed as $R=N^2/L$ and $\phi=Li/N$, (1) can be rewritten as

$$\begin{aligned} \tau &= -\sum_{k=U,V,W} \frac{P}{2}\frac{dR_k}{d\theta}\phi_k^2, \\ i_{in} &= \frac{\Omega}{V_{dc}} \sum_{k=U,V,W} \frac{PR_k}{2}\frac{d\phi_k^2}{d\theta}. \end{aligned} \tag{7}$$

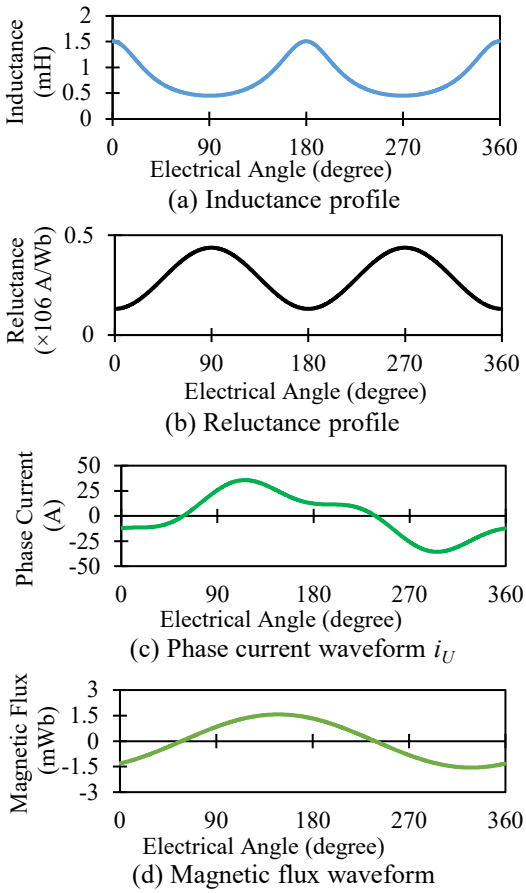

Fig. 4: Operating waveforms of proposed reluctance machine

Equation (7) has the similar form as (2) except that L and i are replaced by R and ϕ, respectively. Therefore, the proposed reluctance machine also results in the constant torque and the constant input current by driving with the sinusoidal flux waveform owing to the sinusoidal reluctance profile, which indicates smaller torque and input current ripples than the SRM similarly to the SynRM. In fact, substituting (6) into (7) yields

$$\tau = -\frac{3P}{4}(R_{\max} - R_{\min})A_p B_p, \quad i_{in} = -\frac{\Omega}{V_{dc}}\frac{3P}{4}(R_{\max} - R_{\min})A_p B_p. \tag{8}$$

In addition to the benefit in the ripple reduction, the proposed reluctance machine does not contain the harmonics in the phase flux waveform. Therefore, the peak magnetic flux can be reduced compared with the SynRM. This implies that the proposed reluctance machine can exhibit greater maximum output torque than the SynRM. Consequently, the proposed reluctance machine can avoid the aforementioned drawbacks of the SynRM and the SRM.

However, it is worth noticing that the phase current waveform of the proposed reluctance machine contains the 3rd harmonics. In fact, the phase current i_U can be calculated according to $Ni_U=R_U\phi_U$ as

$$i_U = \frac{R_{\max} + 3R_{\min}}{4N}A_p\cos\theta + \frac{3R_{\max} + R_{\min}}{4N}B_p\sin\theta - \frac{R_{\max} - R_{\min}}{4N}A_p\cos 3\theta - \frac{R_{\max} - R_{\min}}{4N}B_p\sin 3\theta. \tag{9}$$

Therefore, the proposed reluctance machine does not accept the star-connection of the phase windings. Instead, the proposed reluctance machine should connect the phase windings in the delta-connection. The delta-connection has been avoided in many motors driven with the sinusoidal phase current waveform, including the SynRM, because the undesired circulating current is induced in the phase windings to eliminate the 3rd harmonics in the phase flux waveform, which is not accepted in the delta-connected phase winding. This current results in the deterioration of the torque and input-current ripple, as well as decrease in the efficiency [17]. However, this circulating current in the proposed reluctance machine is natural consequence of the sinusoidal phase flux waveform. Therefore, no undesired current is induced owing to the absence of the 3rd harmonics in the phase flux waveform, which makes the delta-connection acceptable.

By adopting the delta-connection, the 3rd harmonics of the phase current circulates among the phase windings. Therefore, the inverter driving the proposed reluctance machine is required to supply only the 3-phase sinusoidal current without harmonics, as is the same as many conventional electric machines including the SynRM. This indicates that the commercial three-phase inverter can be utilized to drive the proposed reluctance machine.

Simulation

The simulation was carried out to verify the operating principles of the proposed reluctance machine in comparison with the SRM and the SynRM. For this purpose, the driving systems of the proposed reluctance machine, SRM, and SynRM, as shown in Fig 1, were constructed in the model space of the circuit simulator PSIM11.1 (Myway Corp.). In this simulation, the reluctance machines were modeled as the behavior models without considering the power loss and the magnetic saturation. These behavior models were extracted from the two-dimensional magnetic motor models according to the method described in [18].

These magnetic motor models were designed using the FEM-based electromagnetic simulator JMAG18.1 (JSOL Corp.). Figure 5 shows the magnetic motor models. The materials used in the models were listed in Table I. The model of the SRM was designed based on the commercially available SRM, whose specifications were presented in Table II. The other models, i.e. the proposed machine and the SynRM, were designed to have the same stator with the three-phase concentrated windings of 14 turns. Therefore, the only difference among the three motors lies in their rotor geometry.

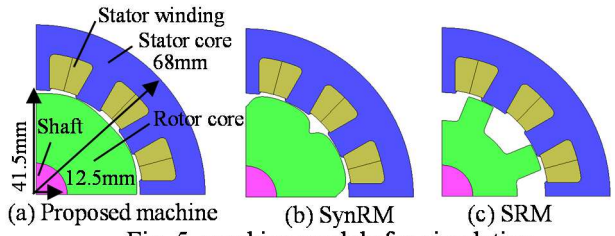

Fig. 5: machine models for simulation

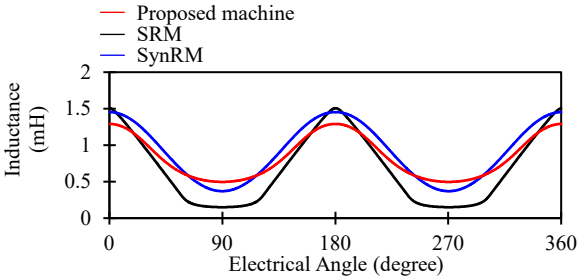

Fig. 6: Inductance profile for simulation

Table I: Material used in FEM model

Component	Material or relative magnetic permeability
Stator	Material name: 35H300 (Nippon Steel Corp.)
Rotor	Material name: 35H300 (Nippon Steel Corp.)
Winding	Relative magnetic permeability: 1
Shaft	Relative magnetic permeability: 1

Table II: Specifications of commercial SRM

Model number	RB165SR-96CSRM (Motion System Tech Inc.)
Rated value	1.2 kW, 96V, 6000 r/min
Pole number	Stator: 12 poles Rotor: 8 poles
Number of turns	14 turns/pole
Min. gap b/w stator and rotor	0.3 mm
Stack length	40 mm

The rotor geometry of the proposed machine and the SynRM were searched so that their reluctance or inductance profiles are sinusoidal and generate the unit value of the torque with minimum possible copper loss under the constraint that the gap between the rotor and the stator is within the range of the gap of the SRM. The rotor geometry search was performed by optimizing the gap at 288 points on the rotor periphery, according to the trial and error approach. Consequently, the inductance profile of each reluctance machine was obtained as shown in Fig. 6.

In the simulation models of the driving systems, the inverter controls the phase current according to the predetermined command value. The phase current command value was calculated according to the theory described in previous sections based on the inductance profiles shown in Fig. 6. The results are shown in Fig. 7. The control diagram of the inverter is shown in Fig. 8. The hysteresis width was set at 0.5A.

In this simulation, the output torque was set at 1 N·m and the rotation speed of the reluctance machines was set at 2000 r/min, which was adopted as typical speed of the vehicle propulsion motors.

The simulation results of the current and flux waveforms were presented in Fig 9(a) and Fig. 9(b), respectively. As can be seen in the figures, the proposed reluctance machine exhibited the smallest peak magnetic flux among the three reluctance machines. This supports that the proposed reluctance machine can output greater output torque under the restriction of the magnetic saturation and therefore improve

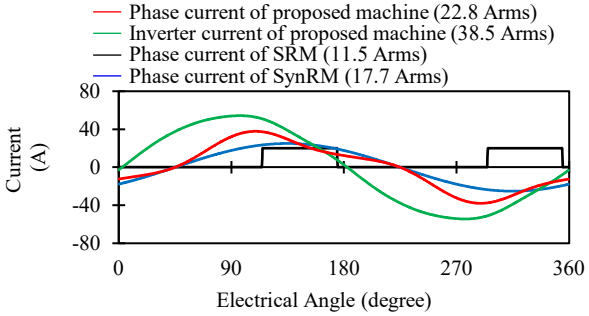

Fig. 7: Phase current command values for simulation

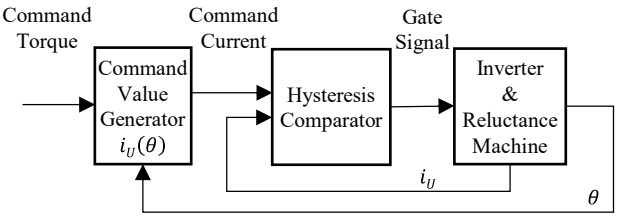

Fig. 8: Control diagram of 3 reluctance machines

the power density of the motor compared with the SynRM. Furthermore, the proposed reluctance machine exhibited the sinusoidal inverter output current despite the 3rd harmonics contained in the phase current waveform, as is expected from the theory.

Figure 9(a) also shows the root-mean-square value of the current waveforms. Among the three reluctance machines, the phase current of the proposed reluctance machine exhibited largest root-mean-square value, indicating the largest copper loss when compared under the same output torque. The reason for this largest phase current is resulted from the smallest peak inductance among the three reluctance machines. In this simulation, the authors could not find the rotor geometry that has the sinusoidal reluctance profile with similar peak inductance as at least the SynRM by only adjusting the rotor periphery geometry. Therefore, this problem may be solved by considering more drastic change in the rotor structure such as introducing the flux barrier structure in the future research.

Considering that the inverter output current of the SynRM is the same as the phase current waveforms, the inverter output current of the proposed reluctance machine is much greater than that of the SynRM. However, this is originated from the fact that the proposed reluctance machine adopts the delta-connection, whereas the SynRM adopts the star-connection. In general, the number of turns of the delta-connected windings should be $\sqrt{3}$ times as large as that of the star-connected windings for driving the motor with the same inverter, although the simulation models have the same number of turns of the phase windings. Therefore, design optimization of the winding turns can be expected to solve this problem, which will be included in the future research.

The simulation results of the torque and input current waveforms are presented in Fig. 9(c) and Fig. 9(d), respectively. As can be seen in the results, the proposed reluctance machine effectively suppressed the torque and input-current ripples compared to the SRM, similarly to the SynRM. These features are consistent with the theory described in the previous sections. Certainly, the small ripples still remain in the torque and input-current ripples in the proposed reluctance machine. The reason for the remaining ripples is unclear. However, these ripples may have caused by small harmonics in the reluctance profile due to insufficient optimization of the rotor geometry. Therefore, these ripples may be further reduced by developing more advanced design optimization technique of the rotor shape. Nonetheless, the

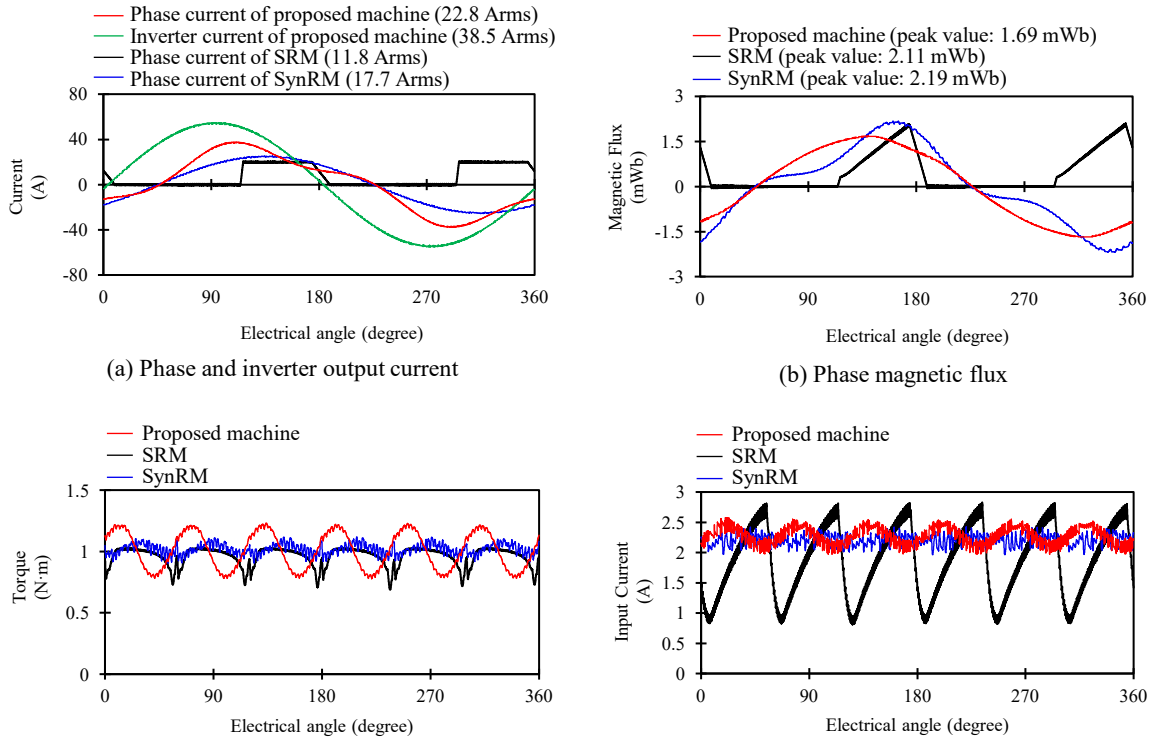

(a) Phase and inverter output current

(b) Phase magnetic flux

(c) Torque

(d) Input current

Fig. 9: Simulation results of operations at 1 Nm, 2000 r/min

simulation results supported the operating principles of the proposed reluctance machine, which suppress the torque and input current ripples with smaller peak magnetic flux.

Experiment

The experiment was also performed to verify the operating principle of the proposed reluctance machine. This experiment evaluates the operating waveforms of the three reluctance machines, i.e. the proposed reluctance machine, the SynRM, the SRM, using the reluctance machine test bench shown in Fig. 10. In this test bench, the reluctance machine under test is mechanically coupled with the induction machine via the instantaneous torque meter and the couplings. The induction machine is utilized as the mechanical load. The reluctance machine under test is supplied with the ac power from the inverter based on the electric circuit illustrated in Fig. 1. The same inverter control was adopted as that utilized in the simulation, which is described in the previous section.

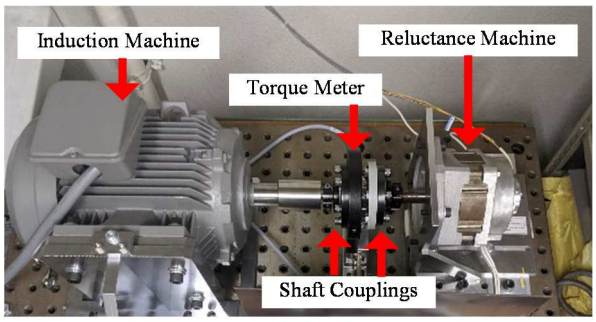

Fig. 10: Machine test bench

The three reluctance machines under test was constructed to have the same stator, similarly as in the simulation. For this purpose, the commercially available SRM of Table I was adopted as the SRM under test; the proposed reluctance machine and the SynRM were constructed by replacing only the rotor of this SRM. Consequently, the three reluctance machines have the three concentrated windings with the same number of turns, although the optimal design of these reluctance machines may require different number of turns according to the winding connection topology. However, the reluctance machines under test are acceptable for this experiment, as the scope of this experiment is to verify the operating principles.

Figure 11 shows the photographs of the rotors of the experimental reluctance machines. These rotors were manufactured to have the rotor periphery geometry of Fig. 5, designed in the previous section. Figure 12 shows the measurement result of the inductance profiles of the three reluctance machines under test. The measurement result exhibited almost the same inductance profiles as the simulation result presented in Fig. 6.

The inverter was operated to output the phase current according to the predetermined command value for the output torque of 1 N·m, which is presented in Fig. 7. For controlling the output current, the inverter was supplied with the DC bus voltage of V_{dc}=96 V. The hysteresis width was set at 5.0A.

In this experiment, the operating waveforms except for the instantaneous torque were observed at the rotation speed of 2000 r/min, whereas only the instantaneous torque waveform was observed at the rotation speed of 100 r/min. The reason for this low rotation speed for torque observation was the limited frequency range of the instantaneous torque meter. Therefore, the input current ripple was measured at 2000 r/min, whereas the torque ripple was measured at 100 r/min.

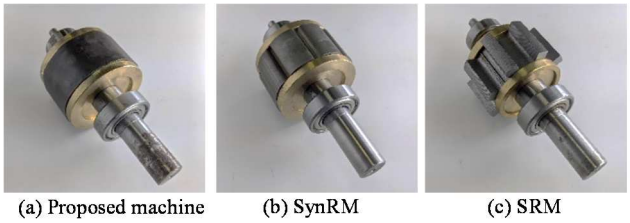

Fig. 11: Photographs of rotors of experimental reluctance machines

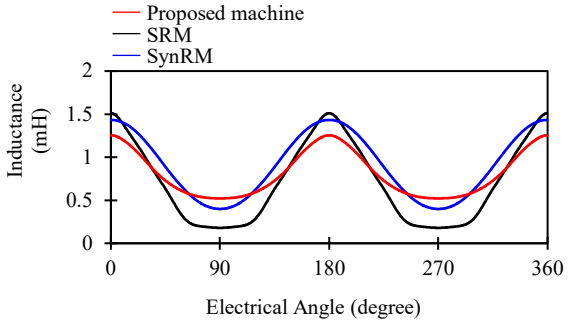

Fig. 12: Measurement results of the inductance profile

Figure 13 shows the experiment results of the operation waveforms. The results indicated that the proposed reluctance machine was successfully driven with the sinusoidal ac current supplied from the inverter and resulted in smaller torque and input-current ripples than the SRM, similarly to the SynRM. These results are consistent with the simulation results as well as the theoretical predictions. Furthermore, the proposed reluctance machine showed the smallest peak magnetic flux among the three reluctance machines, as is consistent with the simulation results. This result suggests that the proposed reluctance machine can improve the power density than the SynRM.

Nonetheless, the input current of the proposed reluctance machine had the largest dc value among the three reluctance machines, which indicates that the proposed reluctance machine exhibited lowest power conversion efficiency. As discussed in the previous section, the reason may lie in the fact that the proposed reluctance machine has the smallest maximum inductance among the three reluctance machines and therefore the proposed reluctance machine needed large root-mean-square value of the phase current to generate the sufficient magnetic flux for the predetermined output torque, i.e. 1 N·m, thus reducing the efficiency. Therefore, in order to improve the efficiency, the optimal design method of the rotor and stator should be investigated to implement the sinusoidal phase reluctance waveform with higher peak inductance. Consequently, the experiment validated the operating principles of the proposed reluctance machine, although the results implied the necessity of advanced rotor and stator design for the proposed machine, which will be investigated in the future research.

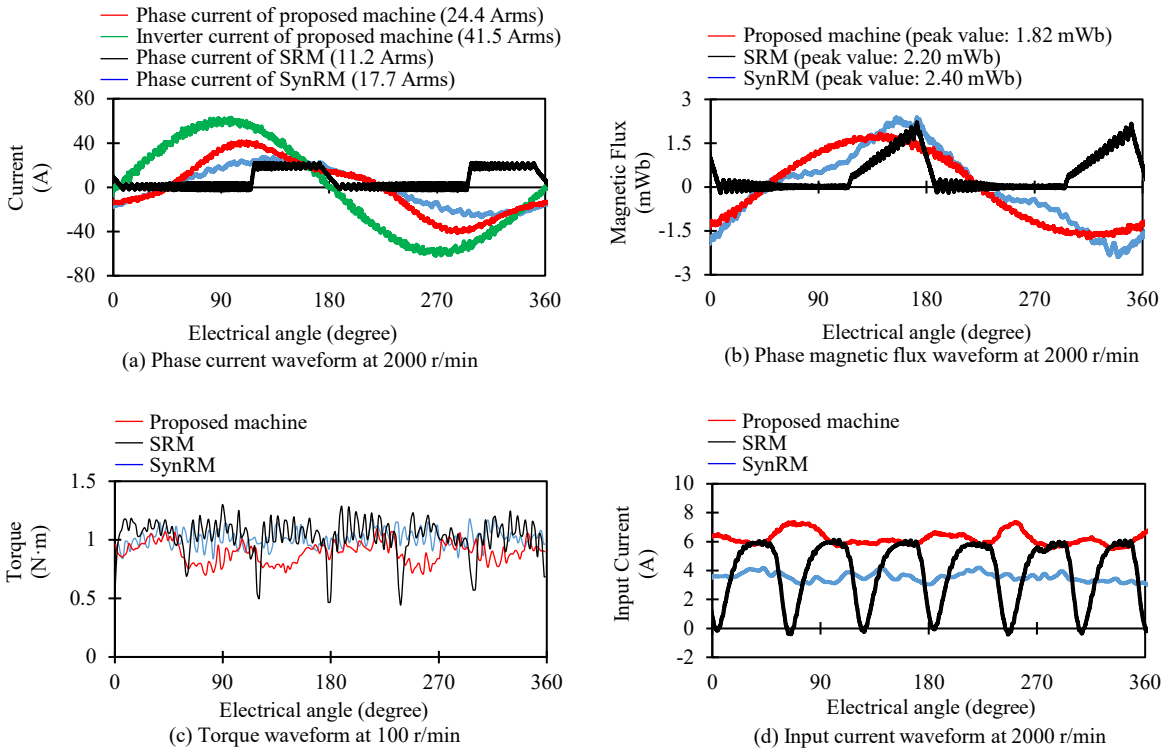

Fig. 13: Experimental results of operating waveforms at 1 Nm

Conclusions

Reluctance machines are attractive for vehicle propulsion owing to simple but robust mechanical construction, high thermal tolerance, and strong cost-effectiveness. However, the conventional reluctance machines such as SRMs and SynRMs are difficult to meet all the three preferable features for the vehicular application: 1. High power density, 2. Low torque and input-current ripples, 3. Being drivable by the normal three-phase inverter. To meet all of these features, this paper proposed a novel reluctance machine having the sinusoidal reluctance profile and driven with the sinusoidal phase flux waveform.

The operating principles of the proposed reluctance machine was evaluated by the simulation and the experiment. As a result, both of the simulation and the experiment supported that the proposed reluctance machine can more satisfies the three features than the SynRM and the SRM, suggesting the feasibility of the proposed machine for vehicle applications.

References

[1] Du J. Wang X., Lu H.: Optimization of magnet shape based on efficiency map of IPSMS for EVs, IEEE Trans. Appl. Supercond, vol. 26, no. 7, pp. 1-7, Oct. 2016, Art no. 0609807.

[2] Jung. H., Park G., Kim D., Jung S.: Optimal design and validation of IPMSM for maximum efficiency distribution compatible to energy comsumption areas of HD-EV, IEEE Trans. Magn., vol. 53, no. 6, pp. 1-4, Jun. 2017, Art no. 8201904.

[3] Hwang Y., Lee J.: HEV motor comparison of IPMSM with Nd sintered magnet and heavy rare-earth free injection magnet in the same size, IEEE Trans. Appl. Supercond., vol. 28, no. 3, pp. 1-5, Apr. 2018, Art no. 5206405.

[4] Zhu Z. Q., Chan C. C.: Electrical machine topologies and technologies for electric, hybrid, and fuel cell vehicles, Proc. IEEE Vehicle Power Propulsion Conf., Harbin, China, pp. 1–6, Sept. 2008.

[5] Raminosoa T. Torrey D. A., El-Refaie A. M., Grace K., Pan D., Grubic S., Bodla K., Huh K.-K.: Sinusoidal reluctance machine with dc winding: an attractive non-permanent-magnet option, IEEE Trans. Ind. Appl., vol. 52, no. 3, pp. 2129-2137, May/Jun. 2016.

[6] Uddin W., Husain T., Sozer Y., Husain I.: Design methodology of a switched reluctance machine for off-road vehicle applications, IEEE Trans. Ind. Appl., vol. 52, no. 3, pp. 2138-2147, May/Jun. 2016.

[7] Martin R., Widmer J. D., Mecrow B. C., Kimiabeigi M., Mebarki A., Brown N. L.: Electromagnetic considerations for a six-phase switched reluctance motor driven by a three-phase inverter, vol. 52, no. 5, pp. 3787-3795, Sept./Oct. 2016.

[8] Bianchi N., Bolognani S., Carraro E., Castiello M.: Electric vehicle traction based on synchronous reluctance motors, IEEE Trans. Ind. Appl., vol. 52, no. 6, pp. 4762-4769, Nov./Dec. 2016.

[9] Zhu J., Cheng K. W. E., Xue X., Zou Y.: Design of a new enhanced torque in-wheel switched reluctance motor with divided teeth for electic vehiles, IEEE Trans. Magn., vol. 53, no. 11, pp. 1-4, Nov. 2017, Art no. 2501504.

[10] Kumar G. V., Chuang C.-H., Lu M.-Z., Liaw C.-M.: Development of an electric vehicle synchronous reluctance motor drive, IEEE Trans. Vehicular Tech., vol. 69, no. 5, pp. 5012-5025, May 2020.

[11] Credo A., Fabri G., Villani M., Popescu M.: Adopting the topology optimization in the design of high-speed synchronous reluctance motors for electric vehicles, IEEE Trans. Ind. Appl., vol. 56, no. 5, pp. 5429-5438, Sept./Oct. 2020.

[12] Payza O., Demir Y., Aydin M.: Investigation of losses for a concentrated winding high-speed permanent magnet-assisted synchronous reluctance motor for washing machine application, IEEE Trans. Magn., vol. 54, no.11, 8207606, 2018.

[13] Suppharangsan W., Wang J.: Experimental validation of a new switching technique for DC-link capacitor minimization in switched reluctance machine drives, Proc. IEEE Int. Electric Machines Drives Conf., Chicago, USA, pp. 1031–1036, May 2013.

[14] Kusumi T., Hara T., Umetani K., Hiraki E.: Phase-current waveform for switched reluctance motors to eliminate input-current ripple and torque ripple in low-power propulsion below magnetic saturation, IET Power Electronics, vol. 13, no. 15, pp. 3351–3359, Nov. 2020.

[15] Kusumi T., Hara T., Umetani K., Hiraki E.: Simultaneous tuning of rotor shape and phase current of switched reluctance motors for eliminating input current and torque ripples with reduced copper loss, IEEE Trans. Ind. Appl., vol. 56, no. 6, pp. 6384–6398, Nov. 2020.

[16] Umetani K., Yamamoto M., Hiraki E.:, Simple flux-based lagrangian formulation to model the non-linearity of concentrated-winding switched reluctance motors , IET Electronics Letters, vol. 51, no. 24, pp.1984–1986, Nov. 2015.

[17] Abramenko V., Petrov I., Nerg J., Pyrhönen J.: Third-order harmonics in synchronous reluctance motors with axially laminated anisotropic rotor and their impact on the motor losses, IEEE Access, vol. 8, pp. 152870-152880, Aug. 2020.

[18] Hara T., Kusumi T., Umetani K., Hiraki E.: A simple behavior model for switched reluctance motors based on magnetic energy, Proc. Intl. Power Electron. Motion Ctrl. Conf. (IPEMC2016), Hefei, China, May 2016.